ELSEVIER

Marine Geology 136 (1997) 245–257

MARINE GEOLOGY
INTERNATIONAL JOURNAL OF MARINE GEOLOGY, GEOCHEMISTRY AND GEOPHYSICS

Stratigraphic numerical modelling of a carbonate platform on the Romanche transverse ridge, equatorial Atlantic

L. Gasperini [a], E. Bonatti [a,b], M. Ligi [a], R. Sartori [c], A. Borsetti [a], A. Negri [c], A. Ferrari [c], S. Sokolov [d]

[a] *Istituto per la Geologia Marina, CNR, Via Gobetti 101, 40100, Bologna, Italy*
[b] *Lamont-Doherty Earth Observatory of Columbia University, Palisades, NY 10964, USA*
[c] *Istituto di Geologia, Università di Bologna, Bologna, Italy*
[d] *Geology Institute, Russian Academy of Science, Moscow, Russia*

Received 18 January 1996; revision 20 September 1996; accepted 20 September 1996

Abstract

The Romanche transverse ridge (equatorial Atlantic) is located in the northern flank of the fracture zone, opposite the eastern ridge-transform intersection (RTI). It constitutes a major positive topographic anomaly that reaches a height of over 4 km above the level predicted by the thermal subsidence curve. A series of E–W aligned peaks, located on the crest of the transverse ridge, were at sea level during early and middle Miocene times; they are presently capped by a ~300 m thick, shallow-water carbonate platform that grew on a subsiding oceanic crust basement surface flattened by erosion at sea level. These structures are now about 1 km below sea level. High resolution seismic reflection surveys and multibeam morphobathymetry as well as study of samples recovered from the carbonate platform allowed a reconstruction of the paleoenvironment and of the vertical movements of the peaks starting from the lower Miocene. Ages derived from microfossils suggest that the base of the carbonate platform dates from 17–25 m.y. ago and the sinking of the platform started between 18 and 13 m.y. ago. These data were included in a numerical simulation model that takes into account thermal and tectonic subsidence, growth potential of the carbonates, subaerial and submarine erosion rates and Mio-Pliocene absolute sea level fluctuations. The results outline the subsidence history of the Romanche transverse ridge and suggest post-Miocene subsidence faster than that predicted by the thermal cooling model.

Keywords: Romanche F.Z.; transverse ridges; shallow water carbonates; subsidence history; numerical modelling

1. Introduction

The Romanche Fracture Zone is the largest among the equatorial Atlantic transforms, offsetting the Mid Atlantic Ridge (MAR) axis by about 950 km (Fig. 1). The main deep valley marking the active part of the transform fault is bound by a system of transverse ridges that are represented by positive topographic anomalies relative to the level predicted by the thermal contraction curve for the oceanic crust. The maximum height of this anomaly (over 4 km) is reached in the northern side of the transform, opposite to the eastern RTI, where a series of three E–W aligned peaks rise to about 1 km below the sea level (Fig. 2). The peaks are capped by shallow water carbonate deposits

PII S0025-3227(96)00068-0

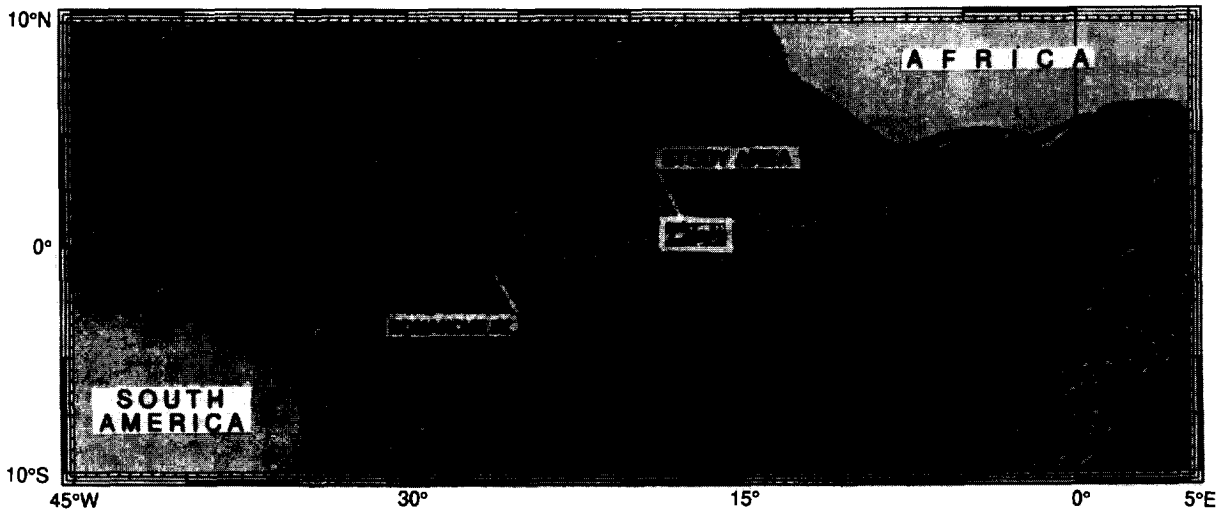

Fig. 1. Satellite-gravity, shaded relief map of the equatorial Atlantic region with the study area indicated (data from Sandwell and Smith, 1992).

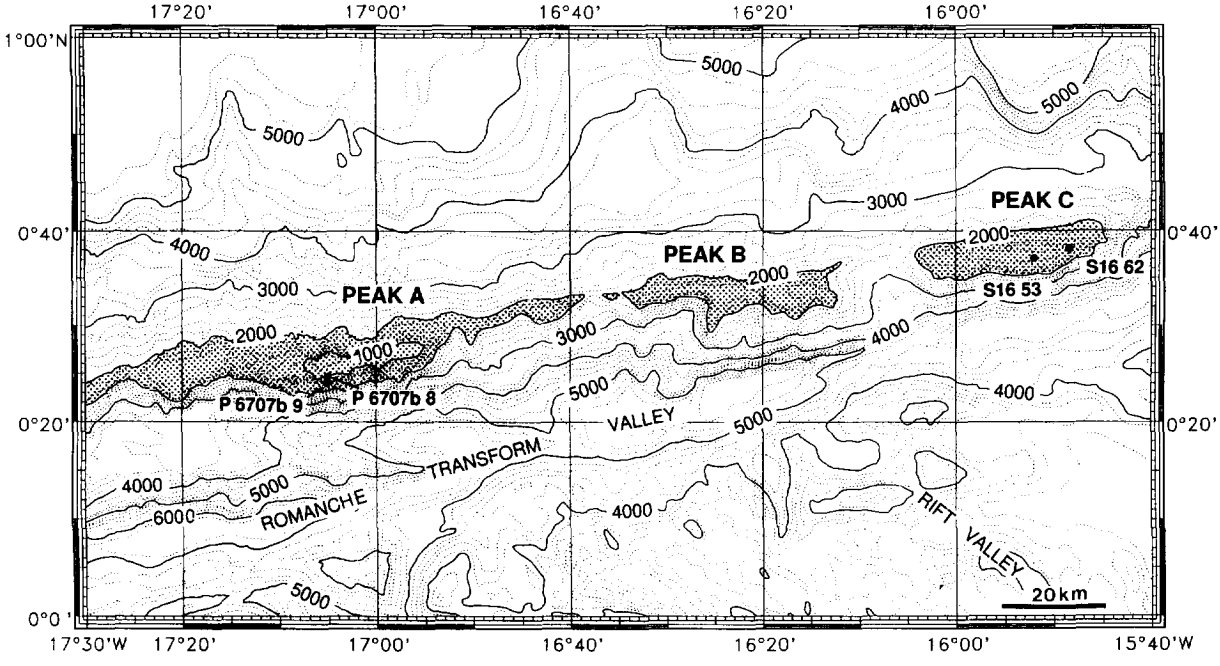

Fig. 2. Bathymetric map showing the three aligned peaks (*A*, *B* and *C*) and the main morphological features of the studied area. Isolines are every 1000 m (thick solid lines) and 200 m (thin solid lines). Rock and sediment sampling stations described in the text are indicated.

formed on top of these structures when they were at sea level. According to Bonatti et al. (1977, 1994a) the transverse ridge is a tectonically uplifted sliver of oceanic lithosphere and its formation is not related to volcanic processes. Single and multichannel seismic reflection lines and

multibeam surveys (Fig. 3) were carried out from 1992 to 1994 during three Italian–Russian joint expeditions on board of *R/V Akademik N. Strakhov*. The techniques that were employed have been described in Bonatti et al. (1994a). Rock and sediment samples were also collected by dredging and gravity coring in these and previous expeditions. This paper reports the results of a stratigraphic and paleoenvironmental analysis of the sedimentary sequence capping the peaks, and discusses the kinematics of the vertical movements of the Romanche transverse ridge.

2. Morphobathymetry

Three peaks rise on the crest of the transverse ridge, labelled from west to east A, B and C (Fig. 2). They are elongated in an E–W direction and the shallowest depth (Peak-A) reaches 900 m bsl. The peaks display a flat top and are separated by N–S striking depressions. The N and S flanks of the transverse ridge are asymmetric, the southern side being steeper. They are dissected by several canyon incisions that may have provided in the past drainage and downslope reworking of the sediments deposited on the upper part of the ridge. A detailed morphological description is possible only for Peak-A, that was investigated with a grid of N–S, close-spaced single channel seismic reflection (Fig. 4) and multibeam lines and with an E–W multichannel seismic reflection line (Fig. 5) located along the crest of the Romanche transverse ridge. We produced from these data a detailed bathymetric map and a 3-D image. The 3-D model (Fig. 6) shows the main stratigraphic units identified by the seismic data and by direct sampling. A shallow-water carbonate platform lies on the sub-horizontal surface of the basement, constituted by oceanic crust. The base of the limestones is located approximately at the same depth in the three peaks suggesting coeval formation; in addition, the thickness of the carbonate units (300–400 m) is similar in the three peaks. A terrace was

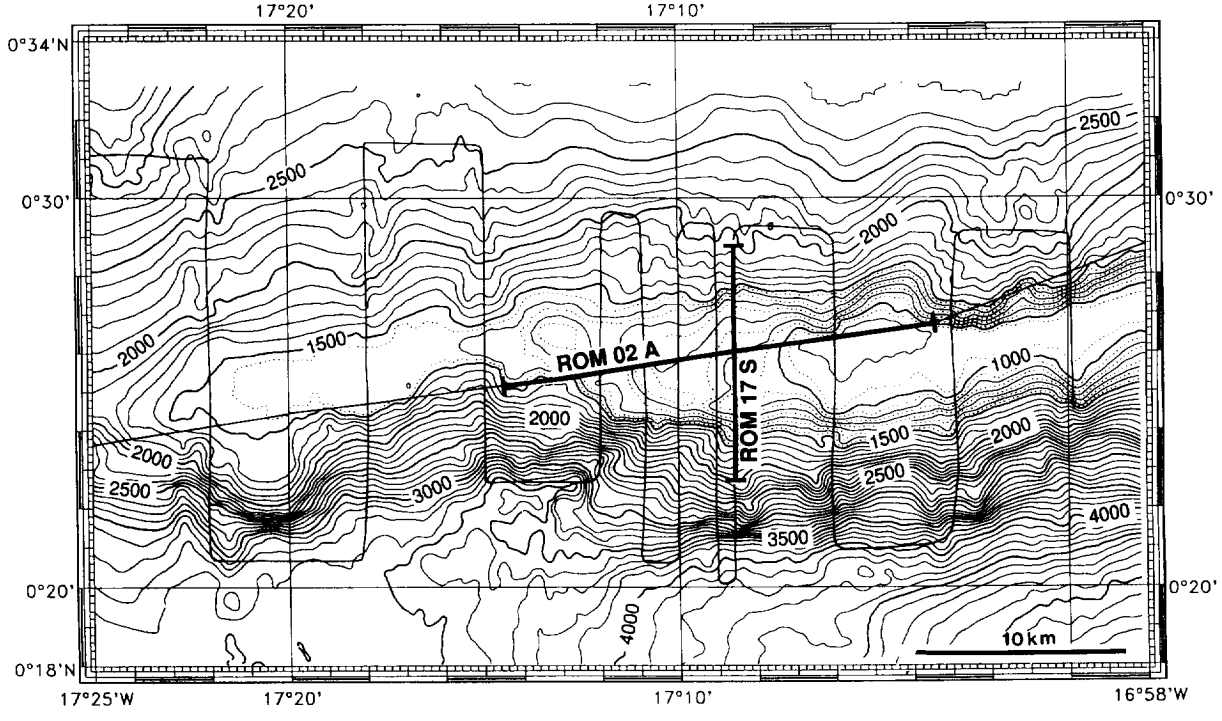

Fig. 3. Detailed bathymetry over peak-A showing the main morphological features. Isolines are every 500 m (thick solid lines), 100 m (thin solid lines) and 50 m (dotted lines). Seismic reflection and multibeam tracks are indicated.

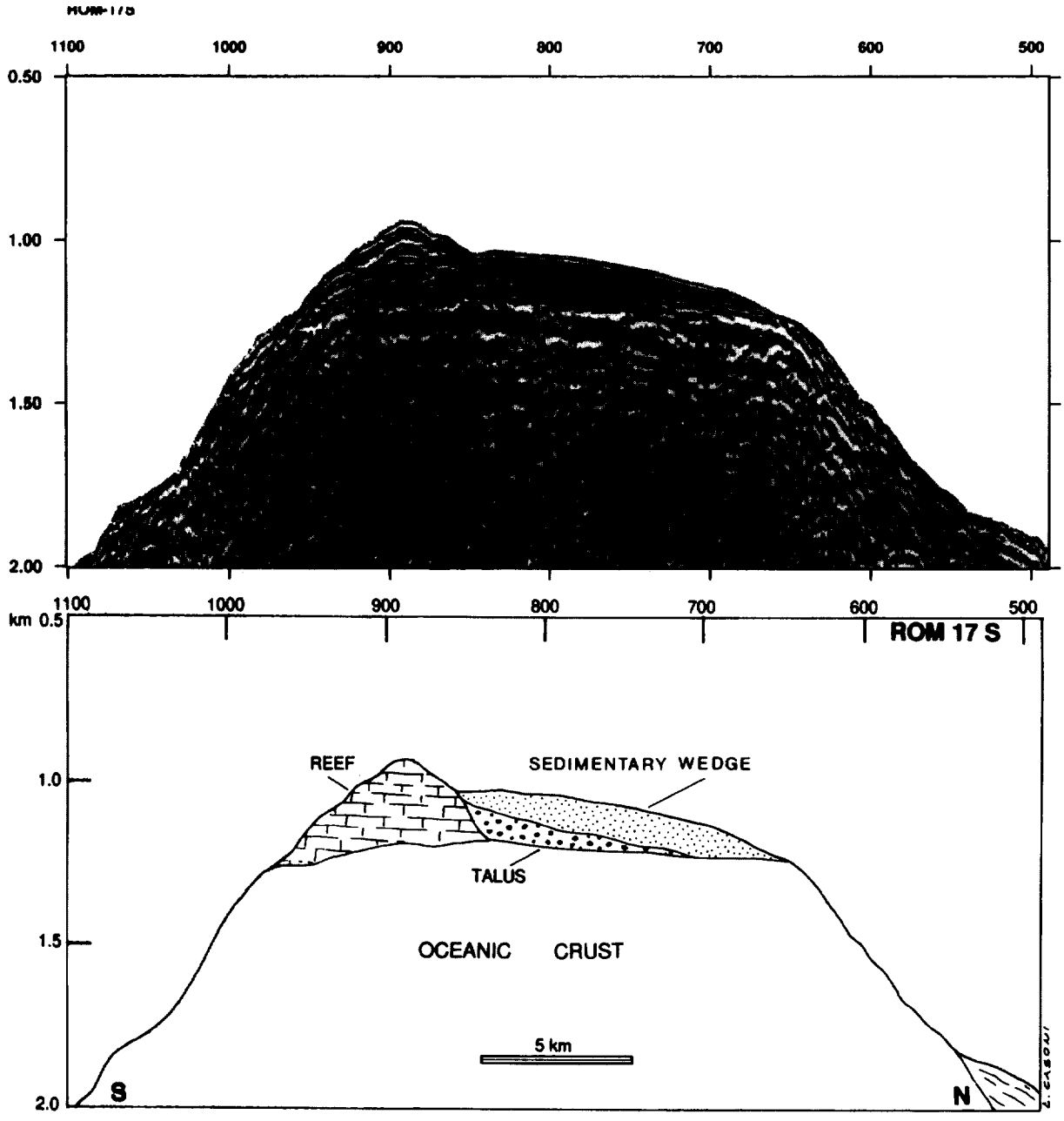

Fig. 4. Segment of single channel seismic line ROM-17 crossing peak A in N–S direction (top). The section has been migrated and depth-converted using the velocity function obtained by the line ROM-2 (Fig. 5). Interpretation line drawing of ROM-17 showing the main seismic units (bottom).

Fig. 5. Portion of the 24 channels time-migrated, depth-converted seismic reflection profile ROM-2 over peak A (ROM-2A)(top). The interval velocities were obtained by averaging stacking velocities within each seismic unit and using Dix's formula. Line drawing (bottom) of the profile showing the main seismic units (see text).

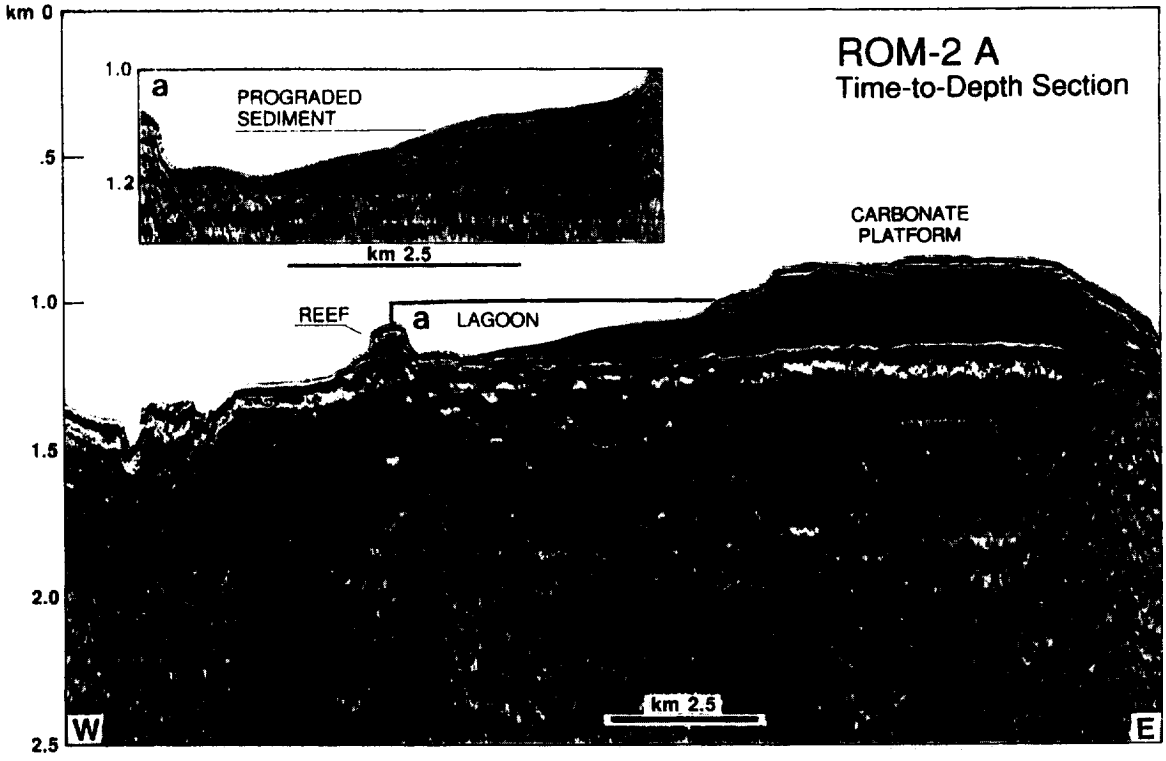
km 0
ROM-2 A
Time-to-Depth Section
1.0
a
PROGRADED
SEDIMENT
.5
1.2
km 2.5
CARBONATE
PLATFORM
1.0
REEF
a
LAGOON
1.5
2.0
km 2.5
W
E
2.5

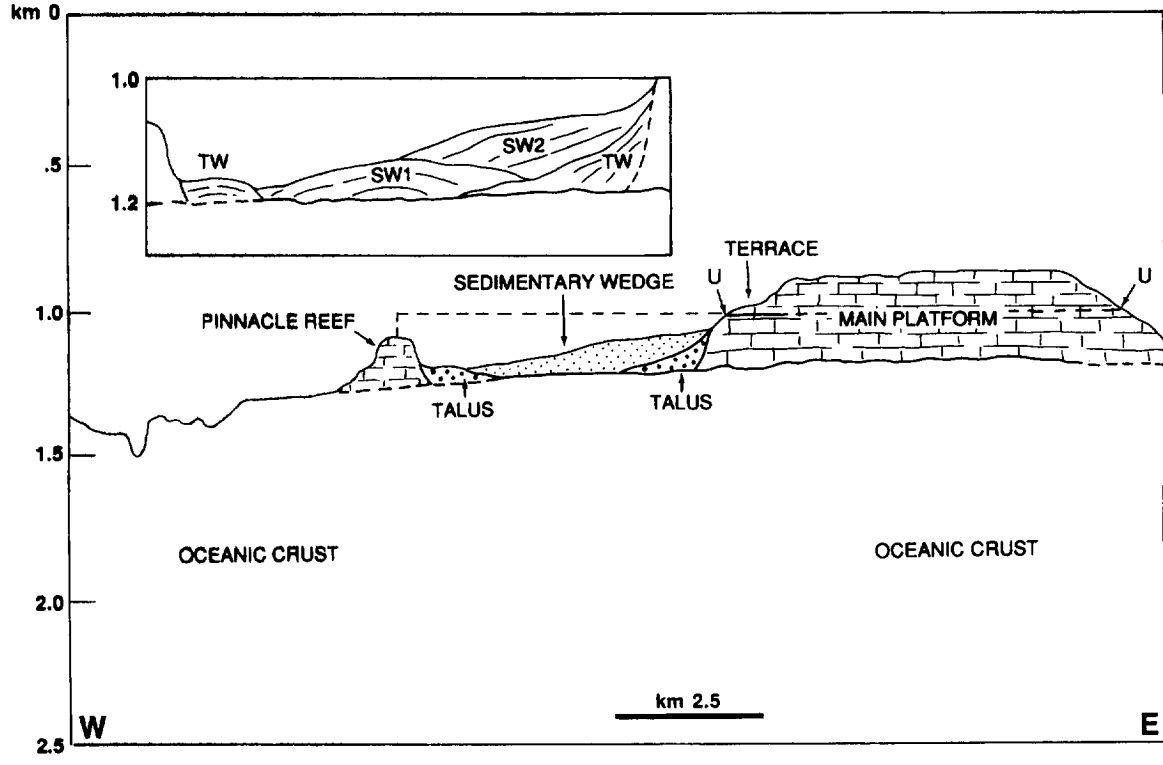
km 0
1.0
TW
SW2
SW1
TW
.5
1.2
TERRACE
SEDIMENTARY WEDGE
U
U
1.0
PINNACLE REEF
MAIN PLATFORM
TALUS
TALUS
1.5
OCEANIC CRUST
OCEANIC CRUST
2.0
km 2.5
W
E
2.5
L. GASPERINI

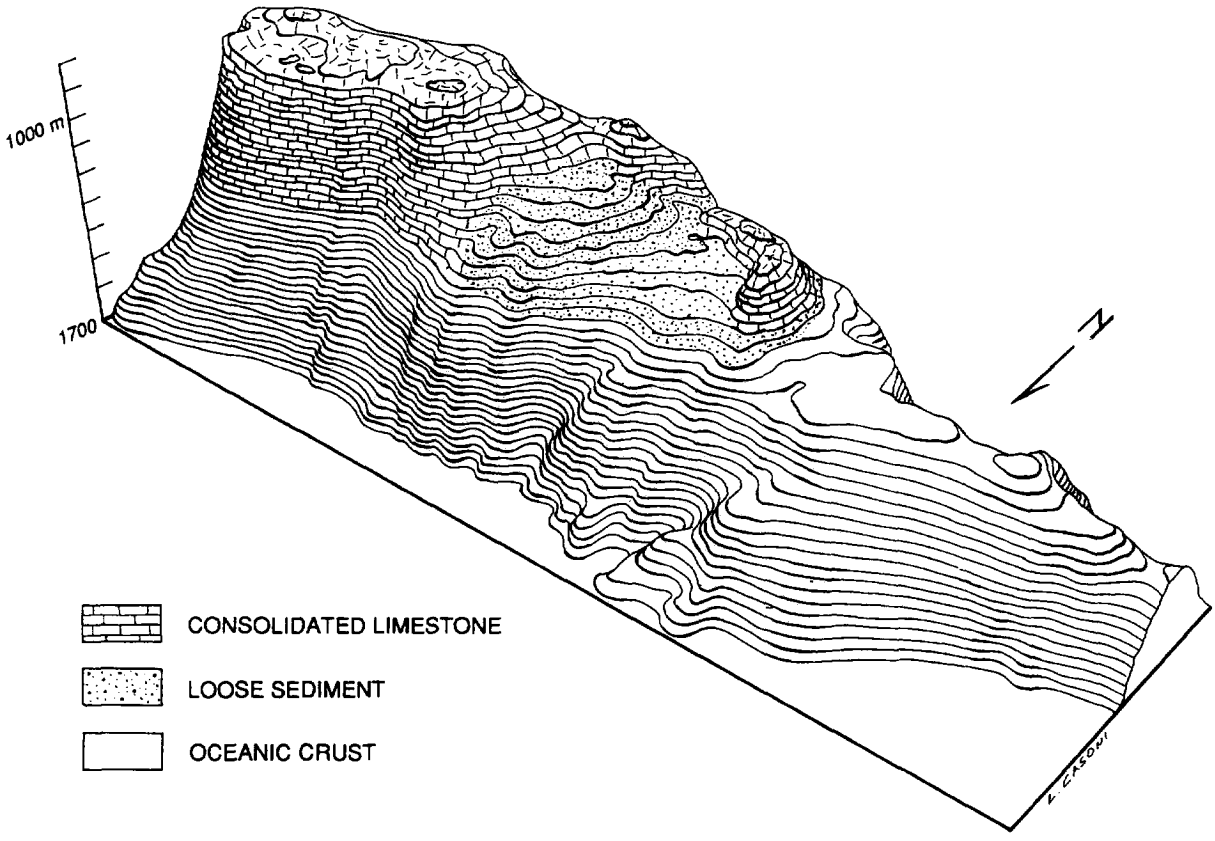

Fig. 6. 3-D model of peak A obtained by multibeam data. Isolines are every 20 m, vertical exageration is ×5 and view is from NNE. The stratigraphic boundaries of the main units were derived from the seismic sections. Note the curve shaped pinnacle reef bounding the lagoon filled by the sedimentary wedge. The western part of the peak is lacking sedimentary units thicker than ~5 m and the oceanic crust is considered cropping out.

observed at the western edge of the Peak-A platform, about 100 m below the top. This terrace marks an erosional surface (Fig. 5) that may have been produced by wave cutting during an episode of relative sea level fall, although we cannot exclude that it represents a scar left by submarine mass wasting of carbonate material along a slide. The main carbonate platform terminates sharply to the west, where it is replaced by a platform-derived sedimentary wedge (Figs. 4 and 5) that formed what appears to have been a lagoon rimmed by a narrow reef barrier (Bonatti et al., 1994a). The reef barrier is nearly semi-circular in shape (Fig. 6) and joins the main platform on the southern side. This reef probably played an important role in the preservation of the sedimentary wedge on top of the peak. Sedimentary wedges of this kind are absent on peaks B and C where barrier reefs were not observed.

3. Seismic stratigraphy

We attempted a stratigraphic reconstruction of the sedimentary sequence capping Peak-A. The stratigraphic framework is based mainly on the geometrical features displayed by the seismic reflection profiles. Thickness estimates are from the depth-converted section ROM-2A (Fig. 5).

We recognised 3 main depositional units:

—The carbonate platform (CP), 300 m thick, consisting of a bioconstructional facies. A ill-

defined unconformity (U) is located about 110 m above the bottom of the unit.

—The Talus Wedge (TW), with a maximum thickness of about 70 m, located at the toe of the carbonate platform and showing very weak or absent internal reflections.

—The Sedimentary Wedge (SW), subdivided into a lower (SW1) and an upper (SW2) subunits. This subdivision appears more clearly when considering the morphology of the sea floor at the sedimentary wedge and the internal reflections of this unit in the migrated seismic section (Fig. 5). We note a light slope-break where SW2 downlaps gently on top of SW1. Both units appear to be well layered but shape and internal geometry are different: SW1 is mound shaped with bi-directional downlap termination of the reflectors; SW2 is wedge shaped and shows offlapping reflectors. The maximum thickness of SW is about 100 m.

Profile ROM-02 crosses the narrow reef barrier, that shows the same acoustic facies of the carbonate platform. Talus deposits similar to those recognised at the toe of the main platform are visible. The height of the pinnacle reef is 140 m; thus, its top is about 160 m deeper than the top of the main platform. The top of the pinnacle reef is approximately at the same level as reflector U (Fig. 5).

4. Rock and sediment samples

Several gravity corings and dredge stations were attempted on the upper part of the three peaks. The corings were mostly unsuccessfull, due to a hard cemented surface found on the sea floor. Only a 1.5 m long core containing an homogeneous, well-sorted foraminiferal ooze was obtained from the sedimentary wedge on Peak-A, implying the presence of pockets of unconsolidated, recent sediments. It represents the very upper part of the succession and is only partially useful for the stratigraphic reconstruction. Limestones were dredged in our and previous expeditions from the three peaks. The stratigraphic and paleofacies analyses are summarized here.

4.1. Peak-A

Dredges P6707b-8 and P6707b-9 (see Fig. 2 for location) were collected in 1967 and some results have been published previously (Bonatti et al., 1977). Samples are heavily phosphatized. Dredge P6707b-9 comes from the basal interval of the carbonate bank and contains an oolitic packstone/grainstone of post late Cretaceous age, as inferred from the occurence of one specimen of the Red Algae *Archeolithotamnium*.

Dredge P6707b-8 is from the top of Peak-A and consists of a phosphatized hardground whose only unequivocal shallow-water element is the hermatypic coral *Stilophora*, that became extinct during Vindobonian time (middle Miocene–early Tortonian).

Ventifact basaltic pebbles, implying subaerial exposure, have been recovered from the western part of Peak-A (Honnorez et al., 1991).

Planktic foraminiferal biomicrites/biosparites capping the shallow water rocks, span the Upper Miocene to Pleistocene (Bolli and Saunders, 1985).

4.2. Peak-C

Dredges S16-53 and S16-62 were collected in 1992 by *R/V Strakhov*. Dredge S16-62, from the base of the bank, is a phosphatized bioclastic packstone containing *Miogypsinae*. The absence of *Miogypsinoides* and *Miogypsinita* would indicate an age ranging between the latest Oligocene and Burdigalian (23–17 m.y. ago approximately). *Stylophora* sp., the hermatypic coral, is also present in some samples with small colonies in a micrite matrix.

Dredge S16-53, from the very top of Peak-C, is heavily phosphatized and contains only *Amphisteginidis* and Red Algae with no stratigraphic value. *Stylophora* is again present (as internal molds) together with another hermatypic coral, *Porites*. The presence of *Stylophora* again indicates that the shallow-water carbonate growth was still active in middle Miocene to early Tortonian times. Very scarce nannoplankton forms have been found in the shallow-water facies. The most characteristic ones are *Calcidiscus*

leptoporus and *Sphenolithus heteromorphus*. *C. leptoporus* FAD is recorded at 18.2 Ma (Gartner, 1992), in the lower part of the NN4 zone of the biostratigraphic scheme proposed by Martini (1971) of late Burdigalian age. *S. heteromorphus* FAD occurs very close to the base of the zone NN4 of Martini (1971) while its LAD defines the top of the Zone NN5 dated at some 13.6 Ma (Gartner, 1992). Stratigraphic constraints inferred from dredges S16-53 and 62 indicate that on Peak C the shallow-water carbonate sedimentation started in the lower Miocene (between 23 and 17 Ma) and ceased in the middle–late Miocene (between 18 and 13 Ma).

Peak-A samples do not give significant stratigraphic constraint. By comparison with Peak-C, presence of *Stylophora* at the top might indicate again that cessation of growth of the carbonate bank occurred in middle–upper Miocene times. No precise indications come from the base where the shallow-water carbonates may have started at the same time as on Peak-C (early Miocene).

5. The numerical model

A simple numerical model was attempted in order to simulate the subsidence history of this portion of the Romanche transverse ridge. The following processes were considered in the simulation: subsidence, carbonate growth, submarine and subaerial erosion, sediment loading and compaction and absolute sea level fluctuations. Peak-A was chosen because it displays the maximum variability of sedimentary facies and the clearest signature of the erosional episodes. The simulation was run also for the other peaks and the results are comparable. We note, however, that reliable stratigraphic data are available only for Peak-C. We assume that Peak-A sediments range within the same time span as those from Peak C.

The model is unidimensional: it aims at reconstructing the evolution of a single stratigraphic column, from the initiation of carbonate deposition to the present-time using steps of 10^3 years.

We considered the following processes.

Subsidence. Oceanic crust subsidence is driven by thermal cooling. The empirical equation of Parson and Sclater (1977) predicts that the top of the oceanic crust deepens relative to sea level according to the square root of age. We considered two different contributions to the subsidence curve, a thermal cooling effect and a tectonic effect assumed to be a linear function of time. The latter assumption was made in order to simplify the interpretation of the model output and because evidences of distinct tectonics phases are lacking. The depth of the basement relative to the present-day sea level was calculated adding at each time step of the simulation the two effects:

$$z(t) = \underset{\text{thermal}}{350[\text{sqrt}(t_0 + t)]} + \underset{\text{tectonic}}{S_{\text{tect}} t}$$

with: z = depth of the oceanic crust at each simulation step expressed in meters; S_{tect} = tectonic subsidence rate expressed in m/Ma; t_0 = age of the oceanic crust at the beginning of simulation, expressed in Ma; t = time expressed in Ma;

In order to compare the effect of each terms, an average estimate of the thermal subsidence rate, expressed in m/Ma, was calculated at the end of each simulation:

$$S_{\text{ther}} = 350[\text{sqrt}(t_0 + \Delta t) - \text{sqrt}(t_0)]/t_{\max}$$

with: Δt = time span of the simulation.

The age of the oceanic crust below the three peaks was calculated assuming a constant ridge/transform geometry and an average spreading rate of 1.75 cm/yr (half rate). This spreading rate is derived from plate kinematic reconstructions of Cande et al. (1988).

Carbonate growth. The carbonate growth potential (G) in a coral reef was assumed to be a function of depth (Chalker et al., 1988), using the following equation (Bosscher and Schlager, 1992):

$$G = G_{\max} \tanh(I_o e^{-kz/I_k})$$

where: $G_{\max}$ = maximum carbonate growth rate (input for the program expressed in mm/yr). I_o = surface light intensity, ranging from 2000 to 2250 mE $m^{-2}s^{-1}$. I_k = saturating light intensity, ranging from 50 to 450 mE $m^{-2}s^{-1}$. k = extinction coefficent, ranging from 0.04 to 0.16 m^{-1}. z = depth, expressed in m. $G_{\max}$ was an input for the program. The amount of carbonate sediment produced was

evaluated at each simulation step. Values typical for equatorial waters were assumed for all the parameters according to Bosscher and Schlager (1992) estimates. Due to the mono-dimensional nature of our simulation model, we considered G_{max} as an average value, neglecting carbonate productivity variation in different domains of the platform.

Marine erosion (ME). Estimates of marine erosion rates in a carbonate platform environment were given by several authors (Hodgkin, 1964; Trudgill, 1976; Spencer, 1985a, b) with a variety of tecniques; we used a range of values of 0.1–10 mm/yr. Marine erosion rate is progressively reduced to zero at an estimate wave base, which was taken to be 10–20 m for all the runs.

Subaerial erosion (SE). Studies on fossil and present-day carbonate banks show that the thickness of calci-turbidite deposits on the flanks of carbonate banks is maximum during interglacials, decreasing significantly in glacial periods (Droxler and Schlager, 1985; Reijmer et al., 1988). This can be due to different causes (dissolution, subaerial cementation, etc..) but data suggest a subaerial erosional rate of carbonate banks not higher than that occurring below sea level. From the literature (Trudgill, 1976; Spencer, 1985a,b; Paulay and McEdward, 1990), we assumed a subaerial erosion rate ranging from 0 to 0.5 mm/yr.

Sediment loading. An estimate of the sedimentary load contribution was attempted assuming a local Airy isostatic compensation (a maximum for the assumption of local compensation). The water-loaded basement depth D_{un} is given by (Steckler and Watts, 1978):

$$D_{un} = T_s[(\rho_m - \rho_s)/(\rho_m - \rho_w)]$$

where T_s is the sediment thickness corrected for compaction; ρ_m (3300 kg/m^3), ρ_w (1000 kg/m^3) and ρ_s are mantle, water and mean sediment column densities. The mean sediment density was assumed to be 1900 kg/m^3 in the initial phase of the modelling. From the beginning of carbonate deposition to the simulation end, the mean sediment density at the j-th step was given by (Sclater and Christie, 1980):

$$\rho_s = \sum_{i=1}^{j} [(\Phi_i \rho_w - (1-\Phi_i)\rho_s^*)/T_s] z_i$$

where Φ_i was the mean porosity of the i-th layer, ρ_s^* the sediment grain density (2710 kg/m^3) and z_i the thickness of the i-th sediment layer.

The porosity of the i-th layer between depth z_1 and z_2 was given by:

$$\Phi_i = \int_{z_1}^{z_2} \Phi(z)\mathrm{d}z/(z_2 - z_1)$$

The assumed porosity/depth function was:

$$\Phi = \Phi_0 \mathrm{e}^{-cz}$$

where Φ_0 (0.67) and c (2.5×10^{-3} m^{-1}) were estimated from areas of similar stratigraphy (Sager et al., 1993).

Compaction. As a new sedimentary layer was added, those below were compacted. If an individual layer between depth z_1' (top) and z_2' (bottom) shifted downwards, the new top depth z_1 was the bottom of the previous layer and the new bottom depth (z_2) was calculated using:

$$z_2 + \Phi_0 \mathrm{e}^{-cz_2}/c + \Phi_0[\mathrm{e}_1^{-cz'} + \mathrm{e}_2^{-cz'} + \mathrm{e}^{-cz_1}]/c + z_1' - z_2' - z_1' = 0$$

Equation above was solved numerically for z_2 using Newton's method.

The present-day basement depth (−1250 m) was the starting point of the simulation and the measured carbonate thickness (300 m) was used to test the fit of the simulation results with observed data. The basement depth was obtained from depth converted seismic reflection line ROM-02 A (Fig. 5). Prior to the simulation, the vertical position of the basement relative to the present datum was calculated, from present to a maximum age of 25 Ma. This procedure was performed going backward in time, considering subsidence (thermal + tectonic) of the basement unloaded by sediment and absolute sea level changes curves (Haq et al., 1988), sampled and linear-interpolated at 10^3 yr steps. Then, by forward modelling (from past to present) the program evaluated the thickness of the sedimentary column, applying carbonate growth, submarine/subaerial erosion functions

and compaction. The depth value necessary to calculate the effect of these processes (functions of depth) was taken iteratively at the immediately preceeding time step. The age range from 25 to 13 m.y. B.P. was explored by the model, given the estimated ages of the samples recovered from the platform. A number of several different combination of the parameters was automatically tested by the program.

6. Discussions

Fig. 7 shows the best-fit output diagram of our simulations i.e., the graphic representation of the subsidence curve for the more realistic combination of the variables ($S_{tect}=0.037$ mm/yr, $G_{max}=2.4$ mm/yr). The x axis shows age increments expressed in Ma. The age range is from present (age = 0) to 21 m.y. ago. The y axis shows depth in meters below present-day sea level; positive values represent emersion episodes. We tested each simulation by checking the agreement between the carbonate thickness calculated by the model and that measured by the seismic reflection depth-converted line (Fig. 5). We start the analysis of the graphic output (Fig. 7) from ~20 Ma, when carbonates began to grow after a period of unknown length of basement erosion at sea level that created the horizontal, flat substratum of the carbonate cap. After a first period of carbonate deposition at sea level, two episodes of subaerial exposure are predicted by the model. Almost the entire carbonate platform was deposited from 20 to ~15.3 Ma; at this time, the model predicts sinking of the platform after an episode of emersion. The previous episode of subaerial exposure produced an unconformity in the carbonate sequence probably marked by an ill-defined reflector laying about 150 m below the top of the carbonate unit (reflector U, Fig. 5).

The last episode of emersion occurred at about 15.3 Ma, assuming the validity of the Haq et al. (1988) global sea level curve. This episode may have represented a very critical phase in the life of the carbonate bank: the bioconstructional activity ceased and the subaerial exposure probably caused karst dissolution and cementation by circulating vadose water. Sea level started rapidly to rise after the last exposure. Absolute sea level rise together with tectonic and thermal subsidence caused rapid sinking of the carbonates and cessation of their growth. Minor relatively positive peaks in the curve never allowed the carbonates to reach again the photic zone where growth is possible. We note that neither absolute sea level changes, nor tectonic and thermal subsidence can explain by themselves the sinking of the carbonate platform, that requires a combination of the two effects, unless other unknown paleo-oceanographic causes are assumed. We also note that a simple thermal effect can not explain the fast total subsidence rate predicted by the model according to the rock samples ages estimates.

Many possible combinations of realistic values of the two main variables S_{tect} and G_{max} were tested in several different simulation sessions but only few of them fit the observations. Estimates of tectonic subsidence rates range between 0.03 and 0.04 mm/yr, starting in an age ranging from 20 to 21 Ma. The estimated average thermal subsidence rate is 0.028 mm/yr considering an actual age of 50 Ma for the oceanic crust underlying the peak-A carbonate platform.

7. Conclusions

The results outlined above lead to the following conclusions:

1. The main carbonate platform was formed by bioconstructional activity between 20 and 15 Ma, which is consistent with the age estimates of the dredged samples.

2. The formation of unit TW is related to the genesis of the carbonate platform. It is probably constituted by relatively coarse carbonate clasts derived from the platform during its active phase. This interpretation is consistent with the lack of internal reflections and the strong acoustic impedance contrast with the overlaying unit marked by a clear reflector.

3. The genesis of the narrow reef barrier is not clear, due to the difference between the depth of its top relative to that of the main platform. The formation of the reef could be coeval to that of

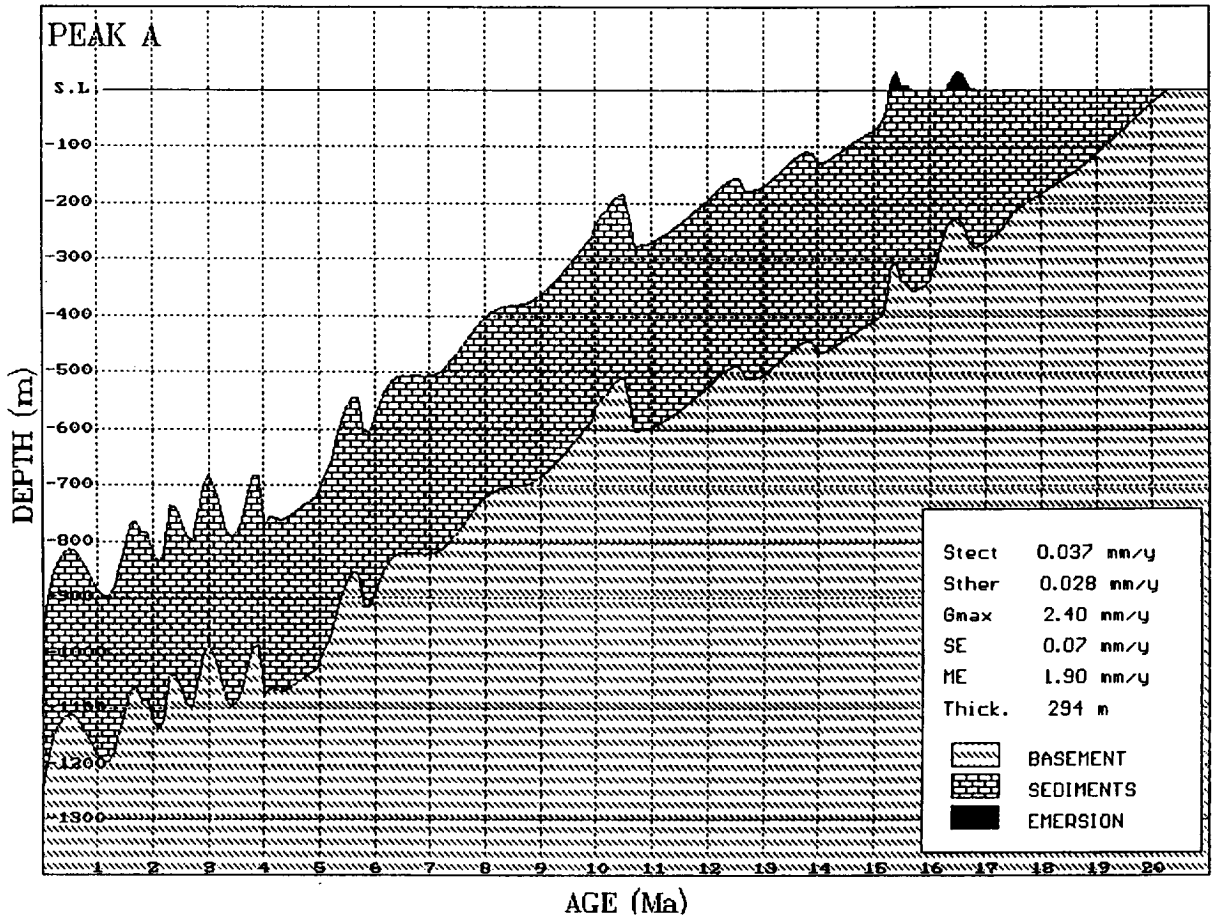

Fig. 7. Simulation model graphic output. The x axis contains ages B.P. expressed in Ma. The legend displays the input values of the variable used in the simulation session: S_{tect} = tectonic subsidence rate; S_{ther} = thermal subsidence rate; G_{max} = maximum carbonate growth rate; SE = subaeriar erosion rate; ME_{max} = maximum submarine erosion rate; *Thick.* = final (present-day) thickness of the carbonate cap.

the main platform if we assume an earlier cessation of carbonate growth on this unit. Assuming a stratigraphic correlation between the top of the pinnacle reef and the internal unconformity (reflector U) within the main platform, we can attribute the cessation of growth of this unit to the episode of subaerial exposure predicted by the model at about 16.5 Ma. Carbonate growth continued on the main platform above the unconformity but not on top of the reef barrier.

4. The unit SW1 was probably deposited during a period of relative low sea-level stand when the top of the platform underwent subaerial erosion. SW1 downlaps on the pinnacle reef talus deposit (Fig. 5), indicating a more recent genesis. SW2 is located landward of SW1 forming a general "backstepping" pattern in the sense of sequence stratigraphy (Posamentier and Vail, 1988). It is also the last depositional unit if we exclude the thin recent foraminiferal ooze draping the whole sedimentary sequence that is outside the seismic vertical resolution. We associate the genesis of SW2 to the last episode of relative sea level rise that marked the final sinking of the platform.

The proposed stratigraphic reconstruction stresses the effects of tectonic and thermal subsidence, and absolute sea level changes in the evolution of the carbonate platform capping the

transverse ridge at the Romanche Fracture Zone. It provide a possible chronostratigraphic framework for the genesis of the observed depositional units. A similar model was also applied to a carbonate platform capping a transverse ridge at the Vema Fracture Zone, in a similar geological setting (Bonatti et al., 1994b). Our estimates of the tectonic subsidence rate contribution, ranging between 0.03 and 0.04 mm/yr, is significantly higher than the estimated thermal cooling rate of subsidence. It implies that mechanisms other than thermal subsidence cause the fast sinking of the transverse ridge and the unusually strong uplift that brought it at and above sea level before 20 Ma. Several possible mechanisms were analysed in previous papers (e.g., Bonatti et al., 1994a). The results stress the importance of transform related vertical tectonics due to transpression and transtension and driven by rearrangement of the plate motion vectors in the Central Atlantic. The stratigraphic study of a Romanche platform, although relative to a limited area, could provide constraints for finer reconstructions of vertical crustal movements and, ultimately, for models on the geodynamic evolution of the equatorial Atlantic.

Acknowledgements

We are very grateful to Captain Leonid Sazonov and the officers and crew of the *R/V N.A. Strakhov* for their skill and cooperation in the field work. Thanks are due to L. Casoni for the drawings and to A. Argnani for the helpful comments and suggestions. This research was sponsored in part by the Italian CNR (Progetto Strategico Mar Rosso/Dorsali). Contribution no. 1052 from Istituto di Geologia Marina, CNR, Bologna.

References

Bolli, H.M. and Saunders, J.B., 1985. Oligocene to Holocene low latitude planktic foraminifera. In: H.M. Bolli et al. (Editors), Plankton Stratigraphy. Cambridge Univ. Press, pp. 155–262.

Bonatti, E., Sarnthein, M., Boersma, A., Gorini, M. and Honnorez, J., 1977. Neogene crustal emersion and subsidence at the Romanche Fracture Zone, Equatorial Atlantic. Earth Planet. Sci. Lett., 35: 369–383.

Bonatti, E., Ligi, M., Gasperini, L., Peyve, A., Raznitzin, Y. and Chen, Y.J., 1994a. Transform migration and vertical tectonics at the Romanche fracture zone, equatorial Atlantic. J. Geophys. Res., 99B11: 779–802.

Bonatti, E., Ligi, M., Gasperini, L., Carrara, G. and Vera, E., 1994b. Imaging crustal uplift, emersion and subsidence at the Vema fracture zone. EOS, 9: 371–372.

Bosscher, H. and Schlager, W., 1992. Computer simulation of reef growth. Sedimentology, 39: 503–512.

Cande, S.C., Labreque, J.L. and Haxby, W.L., 1988. Plate kinematics of the South Atlantic: chron C34 to present. J. Geophys. Res., 93: 13,479–13,492.

Chalker, B.E., Barnes, D.J., Dunlap, W.C. and Jokiel, P.L., 1988. Light and reef building corals. Iterdisc. Sci. Rev., 13: 222–237.

Droxler, A.W. and Schlager, W., 1985. Glacial versus interglacial sedimentation rates and turbidite frequency in the Bahamas. Geology, 13: 799–802.

Gartner, S., 1992. Miocene nannofossil chronology in the North Atlantic, DSDP Site 608. Mar. Micropaleontol., 18: 307–331.

Hodgkin, E.P., 1964. Rate of erosion of intertidal limestone. Z. Geomorphol., 8: 385–392.

Honnorez, J., Mascle, J., Basile, C., Tricart, P., Villeneuve, M. and Bertrand, H., 1991. Margin of a segment of Romanche fracture zone: a morphostructural analysis of a major transform fault of the Equatorial Atlantic ocean. Geology, 19: 795–798.

Haq, B.V., Hardenbol, J. and Vail, P.R., 1988. Mesozoic and Cenozoic chronostratigraphy and cycles of sea level changes. In: Sea Level Changes, an Integrated Approach. SEPM Spec. Publ., 42: 71–95.

Martini, E., 1971. Standard Tertiary and Quaternary calcareous nannofossil zonation. In: A. Farinacci (Editor), Proc. 2nd Planktonic Conf., Rome, 1970. Tecnoscienza, Roma, pp. 739–785.

Parson, B. and Sclater, J.G., 1977. An analysis of the variation of ocean floor bathymetry and heath flow with age. J. Geophys. Res., 82: 803–827.

Paulay, G. and McEdward, L.R., 1990. A simulation model of island reef morphology: the effects of sea level fluctuations, growth, subsidence and erosion. Coral Reefs, 9: 51–62.

Posamentier, H.W. and Vail, P.R., 1988. Eustatic control on clastic deposition, II. Sequence and system tract models. In: C.K. Wilgus et al. (Editors), Sea-Level Changes—An Integrated Approach. SEPM Spec. Publ., 42: 125–154.

Reijmer, J.J.G., Schlager, W. and Droxler, A.W., 1988. ODP site 632: Pliocene–Pleistocene sedimentation cycles in the Bahamian Basin. In: Proc. ODP Sci. Results, 101: 213–220.

Sager, W.W., Winterer, E.L. et al., 1993. Proc. ODP Init. Rep., 143: 111–180.

Sclater, J.G. and Christie, P.A.F., 1980. Continental stretching: an explanation of the post-Mid-Cretaceous subsidence of the post-Mid-Cretaceous subsidence of the central North Sea basin. J. Geophys. Res., 85(B7): 3711–3739.

Spencer, T., 1985a. Marine erosion rates and coastal morphology of reef limestone on Gran Cayman Island, West Indies. Coral Reef, 4: 59–70.

Spencer T., 1985b. Weathering rates on a Carribean reef limestone: results and implications. Mar. Geol., 69: 195–201.

Sandwell, D.T. and Smith, F., 1992. Fall 1992 AGU Meet. Suppl. EOS Trans. AGU, 73, p. 133.

Steckler, M.S. and Watts, A.B., 1978. Subsidence of the Atlantic-type continental margin off New York. Earth Planet. Sci. Lett., 41: 1–13.

Trudgill, S.T., 1976. The subaerial and subsoil erosion of limestones of Aldabra atoll, Indian Ocean. Z. Geomorphol., 26(suppl.): 164–200.